Linear and nonlinear theory of gyroharmonic radiation into modes of a cylindrical waveguide from spatiotemporally modulated electron beams

A. K. Ganguly
Code 6841, U.S. Naval Research Laboratory, Washington, D.C. 20375

J. L. Hirshfield
Omega-P, Inc., 2008 Yale Station, New Haven, Connecticut 06520
and Physics Department, Yale University, Box 6666, New Haven, Connecticut 06511
(Received 7 January 1993)

Linear and nonlinear theory is presented for the generation of gyroharmonic radiation from spatiotemporally modulated electron beams in cylindrical waveguides. Selection rules for axisymmetric beams are derived that show coupling at the mth temporal harmonic to be absent for all TM modes, and for TE modes other than those with an azimuthal mode index of m. Estimates from linear theory are given for the effects of spreads in axial momentum and guiding-center radius. A nonlinear multimode theory is developed in order to treat mode saturation and mode competition for TE modes in a down-tapered guide magnetic field. Numerical simulations of the multimode nonlinear generation of fifth-harmonic radiation at 94 GHz from a 150-kV, 6.667-A, $\alpha=2$ beam show that nearly 90% of the initial transverse energy of the beam can be converted to fifth-harmonic radiation in the TE_{51} mode, and that less than 2.5% of the beam energy is converted to other harmonics. Use of a linearly tapered guide magnetic field gives lower saturated fifth-harmonic conversion efficiency than does use of a nonlinear taper. But the linear-taper case shows greater resilience to axial momentum spread than does the nonlinear taper case. The spent beam is nearly monoenergetic and phase coherent at saturation, suggesting that overall harmonic-conversion efficiencies can approach 100% if a single-stage depressed collector is used to recover the spent beam energy.

PACS number(s): 52.40.Mj, 52.75.Ms, 41.60.Ap

I. INTRODUCTION

Linear analysis of the coupling between a spatiotemporally modulated electron beam and the fields of a rectangular waveguide has recently been published [1,2]. This work showed that cumulative exchange of transverse beam energy into electromagnetic radiation can occur at frequencies that are harmonics of the beam modulation frequency, provided certain selection rules and matching conditions are observed. This analysis suggested that a class of devices can be contemplated to furnish radiation at frequencies and power levels that have not yet been reached with more conventional devices, such as klystrons [3] and gyrotrons [4]. Applications for such novel radiation sources could include drivers for next-generation electron-positron colliders [5], sources for fusion plasma heating and control [6], and oscillators for advanced radar systems [7].

The harmonic conversion process examined in Refs. [1] and [2] is fundamentally different from processes underlying other gyroresonant interactions, such as the electron cyclotron maser (ECM) [8], the cyclotron autoresonance maser (CARM) [9], the slow-wave cyclotron amplifier (SWCA) [10], the peniotron [11] or the wiggler-free free-electron laser (FEL) [12]. In the ECM, azimuthal phase bunching is induced by the relativistic interaction of gyrating particles with fast-wave fields near the gyrofrequency or one of its harmonics. In the CARM, a combination of azimuthal phase bunching and axial spatial bunching is induced by the relativistic interaction of gyrating particles with fast-wave fields near the Doppler-shifted gyrofrequency. In the SWCA, axial spatial bunching is induced by the relativistic interaction of gyrating particles with slow-wave fields near the Doppler-shifted gyrofrequency. In the peniotron no bunching is produced, but the guiding centers of large-orbit gyrating particles drift in a nonrelativistic interaction with fast-wave azimuthally varying fields, and give up transverse momentum, whatever the value of the initial particle phase. In the wiggler-free FEL, a time-independent helical variation on the electron beam allows coupling between fast or slow electromagnetic waves and slow beam modes, with gain occurring at the Doppler-shifted gyrofrequency. In a linearized description of any of these interactions, power flow into the fields is a process *second-order* in the amplitude of the wave fields, since the perturbed current density $\mathbf{J}_1(\mathbf{r},t)$ is proportional to the electric field $\mathbf{E}_1(\mathbf{r},t)$ and the power flow is calculated from $\mathbf{J}_1(\mathbf{r},t)\cdot\mathbf{E}_1(\mathbf{r},t)$. Consequently, the logarithmic decrement of the power flow is independent of the field amplitude, and a linearized dispersion relation can be found that governs the wave growth and refraction.

In contrast, the harmonic-conversion process requires neither induced phase and/or spatial bunching nor induced orbit drifts, since power flow to the fields is a *first-order* process. The electron beam is taken as having been prepared (prior to the interaction) so that its equilibrium current density $\mathbf{J}_0(\mathbf{r},t)$ carries spatiotemporal modula-

1063-651X/93/47(6)/4364(17)/$06.00

tion. In this case, the lowest-order contribution to the power flow into the fields is calculated from $\mathbf{J}_0(\mathbf{r},t)\cdot\mathbf{E}_1(\mathbf{r},t)$. The concept of a linearized dispersion relation has no meaning in this case. These ordering arguments were made by Kou *et al.* [13] in connection with a calculation of fields induced in a cavity by temporally modulated beams. Indeed, it is well known that a first-order process governs small-signal power flow in the output cavity of multicavity klystrons. A traveling-wave gyro-interaction in which spatiotemporal features on the beam govern power flow into the fields occurs in the so-called "gyrotwystron" [14,15], although to date this device has been considered only as an amplifier, rather than a harmonic converter. Of course, spatiotemporal modulation on a beam is related to the rf field strength in the structure where the beam was prepared, so the overall order of the radiation process is not strictly first order in E alone.

Linear theory as presented in Refs. [1] and [2] is only competent to describe the small-amplitude behavior of the harmonic-conversion process. But conceptual arguments suggest that conditions may be found where the beam electrons remain in phase with the propagating radiation fields and continuously lose transverse energy, although the rate of energy loss may become vanishingly small as the transverse energy approaches zero. Clearly, an accurate description of such a process requires a nonlinear theory. Moreover, when several radiation modes of a waveguide can interact simultaneously with the beam electrons, a nonlinear superposition of all the interacting modes must be taken into account. Furthermore, since a down-tapered guide magnetic field is essential to maintain phase synchrony between the particles and the fields, nonlinear orbit equations must be used to find the combined effects of rf electromagnetic and static radial magnetic fields upon the power flow process. This paper is intended to address these issues by introducing a multimode slow-time-scale formulation of the electromagnetic fields and the exact nonlinear particle orbit equations in a mutually coupled interaction. The theory is formulated for TE and TM modes in cylindrical waveguides (rather than only for TE modes in rectangular waveguides as in Refs. [1] and [2]); this turns out to avoid a plethora of waveguide modes that might be capable of coupling simultaneously to a spatiotemporally modulated beam. The theory takes into account spread in orbit pitch angle and center of gyration. An abbreviated report of the nonlinear theory has been published previously [16].

This paper is organized as follows. Section II is devoted to development of the linear theory for harmonic conversion from a spatiotemporally modulated beam into TE and TM modes of a cylindrical waveguide. A general formulation is given in Sec. II A that includes the effects of pitch-angle and center-of-gyration spreads in the electron beam, and conditions are found that limit significantly the number of waveguide modes that can accept power from the beam. Section II B gives results for an idealized axisymmetric "cold" beam, i.e., one in which all electrons have identical momenta and centers of gyration. Section II C provides a calculation of the diminution in power transfer from the beam to a designated waveguide mode arising in the linear regime from a spread in particle axial momentum. Section II D gives an estimate for the rate of power flow into TE modes other than the design mode in the linear regime, and gives examples of mode competition for a conceptual device designed to operate at the fifth gyroharmonic at 94 GHz. Section III contains the nonlinear slow-time-scale multimode formulation for TE and TM modes, which is specialized to the case of interactions with a spatiotemporally modulated beam. Section IV describes development of a nonlinear simulation code based on the theory of Sec. III, gives numerical nonlinear results for fifth-harmonic conversion as discussed in a linear context in Sec. II D, and also gives numerical results for the power flow into competing modes. Section V contains conclusions drawn from this work and suggestions for further study.

II. LINEAR THEORY

A. Basic formalism

The first-order interaction between a beam possessing spatiotemporal modulation and the fields of a cylindrical waveguide can be characterized along lines similar to those employed previously [1,2] for rectangular waveguides. The basic idea is to calculate $dP(z,t)/dt$, the spatial rate of change along z of the instantaneous wave power, from the work done by the beam particles on the fields. The fields are assumed to be those for a uniform empty waveguide, but with a slowly varying electric-field amplitude $E_0(z,t)$. The particle trajectories are assumed to be unaffected by the fields in such a linear first-order analysis. A second expression for $dP(z,t)/dt$ can also be found from the usual Poynting relationship between $P(z,t)$ and the fields. Equating the two expressions allows an equation for $dE_0(z,t)/dz$ to emerge. This is then averaged over the time of interaction $T=z/v_z$ for particles of axial velocity v_z coupling to the wave over a distance z, and the resulting time-averaged value $dE_0(z)/dz$ can then be integrated over z out to the total interaction length L to find $E_0(L)$ in terms of the input value $E_0(0)$ and the beam parameters. Since growth of the wave fields can be determined in this manner from the zeroth-order beam parameters, rather than from a first-order induced current (as is customary in linear analysis of most wave-particle interactions), the coupling is first order, rather than second. These ordering arguments were made previously by Kou *et al.* [13], although significant differences exist between that calculation and what is presented in this paper; these differences will be discussed below.

In general, we consider a class of electron beams having a current density $\mathbf{J}(\mathbf{r},t)$ that can be characterized by the momentum-space integral

$$\mathbf{J}(r,\theta,z,t)=-e\int_{-\infty}^{\infty}du\int_0^{\infty}dw\,w\int_0^{2\pi}d\varphi\left[\hat{\mathbf{e}}_\phi\frac{w}{\gamma}+\hat{\mathbf{e}}_z\frac{u}{\gamma}\right]\times\delta(\phi-\phi_0+\xi z-pt)f_0(u,w,\varphi,r,\theta)\ , \quad (1)$$

where r and θ are the radial and azimuthal coordinates, and u and w are components of a beam electron's momentum (divided by the electron rest mass m) along and across the z axis. The relativistic Lorentz factor is related to the momenta by $\gamma^2=(u^2+w^2+c^2)/c^2$. A uniform static magnetic field $\hat{\mathbf{e}}_z B_0$ is imposed. Unit vectors $\hat{\mathbf{e}}_\phi$ and $\hat{\mathbf{e}}_z$ are along the angular and axial momenta of the gyrating particles. (The lowest-order particle orbits have no motion along their radii of gyration.) The distribution function for the beam electrons is given by $f_0(u,w,\varphi,r,\theta)$, where φ is the azimuth angle in momentum space. The various coordinates are shown in Fig. 1.

The δ function in the integrand of Eq. (1) gives the equilibrium current density its spatiotemporal character: an individual particle moves on a helix of axial pitch number ξ, and the helix rotates with an angular frequency p. When the electrons are injected adiabatically along a slowly tapered magnetic field from an ideal cyclotron autoresonance accelerator driven at angular frequency p, it is shown in Ref. [1] that $\xi=\gamma(p-\Omega)/u$, where $\Omega=eB/m_0\gamma$ is the gyrofrequency in the uniform region after the taper.

The instantaneous rate of power transfer from the beam to the fields is given by

$$\frac{dP(z,t)}{dz}=-\int_0^R dr\, r\int_0^{2\pi} d\theta\, \mathbf{J}(r,\theta,z,t)\cdot\mathbf{E}(r,\theta,z,t)\ , \tag{2}$$

where $\mathbf{J}(r,\theta,z,t)$ is given by Eq. (1), and where R is the waveguide radius. The electric fields of an empty uniform cylindrical waveguide are given by

$$E_r(r,\theta,z,t)=E_0(z,t)\left[\frac{m}{k_\perp r}\right]J_m(k_\perp r)\sin\Theta_m \tag{3a}$$

and

$$E_\theta(r,\theta,z,t)=E_0(z,t)J'_m(k_\perp r)\cos\Theta_m \tag{3b}$$

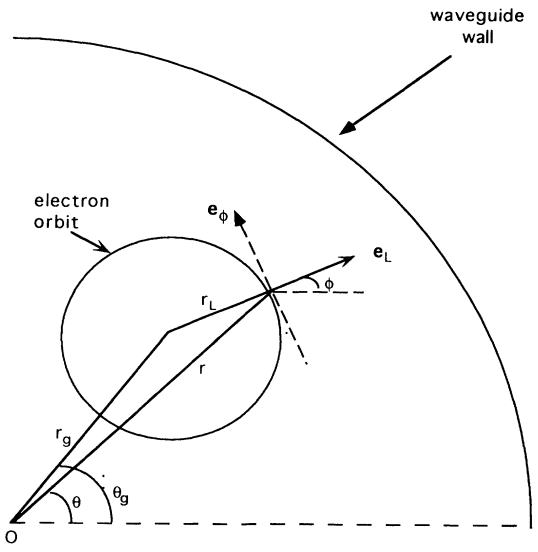

FIG. 1. Coordinate system.

for TE_{mn} modes, and by

$$E_r(r,\theta,z,t)=E_0(z,t)\left[\frac{k_z}{k_\perp}\right]J'_m(k_\perp r)\cos\Theta_m\ , \tag{4a}$$

$$E_\theta(r,\theta,z,t)=-E_0(z,t)\left[\frac{k_z}{k_\perp}\right]\left[\frac{m}{k_\perp r}\right]J_m(k_\perp r)\sin\Theta_m\ , \tag{4b}$$

and

$$E_z(r,\theta,z,t)=E_0(z,t)J_m(k_\perp r)\sin\Theta_m \tag{4c}$$

for TM_{mn} modes. In Eqs. (3) and (4), $\Theta_m=m\theta+k_z z-\omega t$, and the forms given are for circularly polarized waves with right-hand rotation for $\omega>0$ and left-handed rotation for $\omega<0$. The function $J_m(s)$ is the Bessel function of the first kind; $J'_m(s)=(d/ds)J_m(s)$; $k_\perp R=s'_{mn}$ for TE_{mn} modes and $k_\perp R=s_{mn}$ for TM_{mn} nodes, where s'_{mn} is the nth zero of $J'_m(s)$ and s_{mn} is the nth zero of $J_m(s)$. The amplitude $E_0(z,t)$ is slowly varying with both z and t such that $k_z^{-1}d[\ln E_0(z,t)]/dz\ll 1$ and $\omega^{-1}d[\ln E_0(z,t)]/dt\ll 1$.

In order to carry out the integrations in Eq. (2), it is convenient to transform the fields given by Eqs. (3) and (4) from spatial coordinates (r,θ) to (r_L,ϕ,r_g,θ_g), where $r_L=w/\Omega\gamma$ is the gyration radius, and r_g and θ_g are the radial and azimuthal coordinates of the center of gyration. These quantities are related by $r^2=r_g^2+r_L^2+2r_g r_L\cos(\phi-\theta_g)$. This procedure, rather commonly undertaken in the theory of gyroresonant interactions, has recently been clearly elucidated by Zhang [17], who employed Graaf's addition theorem [18]

$$J_m(k_\perp r)e^{im(\theta_g-\theta)}=\sum_{j=-\infty}^{\infty}J_{m+j}(k_\perp r_g)J_j(k_\perp r_L)e^{ij(\theta_g-\phi)}$$

to find the following results for the TE_{mn} modes:

$$E_L(r_L,\phi,r_g,\theta_g,z,t)=E_0(z,t)\sum_{j=-\infty}^{\infty}J_{m-j}(k_\perp r_g)\times\left[\frac{1}{k_\perp r_L}\right]J_j(k_\perp r_L)\sin\Xi_{mj} \tag{5a}$$

and

$$E_\phi(r_L,\phi,r_g,\theta_g,z,t)=E_0(z,t)\sum_{j=-\infty}^{\infty}J_{m-j}(k_\perp r_g)J'_j(k_\perp r_L)\times\cos\Xi_{mj}\ , \tag{5b}$$

where $\Xi_{mn}=(m-j)\theta_g+j\phi-\omega t+k_z z$, $E_L=\mathbf{E}\cdot\hat{\mathbf{e}}_L$ and $E_\phi=\mathbf{E}\cdot\hat{\mathbf{e}}_\phi$. Similar procedures give the fields for the TM_{mn} modes to be

$$E_L(r_L,\phi,r_g,\theta_g,z,t)=E_0(z,t)\frac{k_z}{k_\perp}\sum_{j=-\infty}^{\infty}J_{m-j}(k_\perp r_g)\times J'_j(k_\perp r_L)\cos\Xi_{mj}\ , \tag{6a}$$

$$E_\phi(r_L,\phi,r_g,\theta_g,z,t)$$

$$=E_0(z,t)\frac{k_z}{k_\perp}\sum_{j=-\infty}^{\infty}J_{m-j}(k_\perp r_g)\left[\frac{1}{k_\perp r_L}\right]$$

$$\times J_j(k_\perp r_L)\sin\Xi_{mj}\ , \tag{6b}$$

and

$$E_z(r_L,\phi,r_g,\theta_g,z,t)=E_0(z,t)\sum_{j=-\infty}^{\infty}J_{m-j}(k_\perp r_g)J_j(k_\perp r_L)$$

$$\times\sin\Xi_{mj}\ . \tag{6c}$$

To carry out the configuration- and momentum-space integrals in Eqs. (1) and (2), we invoke the identity

$$r dr\, d\theta\, du\, dw\, d\varphi = r_g dr_g d\theta_g du\, dw\, d\phi\ , \tag{7}$$

which follows from finding the Jacobian for the coordinate system transformation [17]. As a result, Eq. (2) can be written as

$$\frac{dP(z,t)}{dz}=-eE_0(z,t)$$

$$\times\int dr_g r_g\int d\theta_g\int du\int dw\frac{w}{\gamma}\int d\phi\, f_0(r_g,\theta_g,u,w,\phi)\delta(\phi-\phi_0+\xi z-pt)$$

$$\times\sum_{j=-\infty}^{\infty}J_{m-j}(k_\perp r_g)\times\begin{cases}wJ_j'(k_\perp w/\Omega\gamma)\cos\Xi_{mj} & \text{(8a)}\\ (j\Omega\gamma k_z/k_\perp^2-u)J_j(k_\perp w/\Omega\gamma)\sin\Xi_{mj}\ , & \text{(8b)}\end{cases}$$

where Eq. (8a) applies to TE_{mn} modes and Eq. (8b) to TM_{mn} modes. [Below, through Eqs. (15a) and (15b), the (a) and (b) versions of each equation will apply in the same manner to TE_{mn} and TM_{mn} modes, respectively.]

Equations (8a) and (8b) show, for a beam with sufficient azimuthal symmetry in its distribution of guiding centers, that a powerful selection rule can emerge. If the overall distribution function $f_0(r_g,\theta_g,w,u,\phi)$ can be written as a separable function $g_0(r_g,w,u,\phi)h_0(\theta_g)$ and if $h_0(\theta_g)=\sum_q[a_q\cos(q\theta_g)+b_q\sin(q\theta_g)]$, then the only terms under the summations in Eqs. (8a) and (8b) that have nonzero values after integration over θ_g are those for which $m-j=q$. In particular, for an azimuthally symmetric beam with $q=0$, all terms after integration are zero except for the $j=m$ term, for which Eqs. (8a) and (8b) become

$$\frac{dP(z,t)}{dz}=-2\pi eE_0(z,t)$$

$$\times\int dr_g r_g J_0(k_\perp r_g)\int du\int dw\frac{w}{\gamma}\int d\phi\, g_0(r_g,w,u,\phi)\delta(\phi-\phi_0+\xi z-pt)$$

$$\times\begin{cases}wJ_m'(k_\perp w/\Omega\gamma)\cos\Phi_m & \text{(9a)}\\ (m\Omega\gamma k_z/k_\perp^2-u)J_m(k_\perp w/\Omega\gamma)\sin\Phi_m\ , & \text{(9b)}\end{cases}$$

where $\Phi_m=m\phi-\omega t+k_z z$. We shall henceforth limit the discussion to beams that are axisymmetric in their angular distributions of both guiding center and momentum. It is furthermore plausible to assume that the overall distribution function can be taken to be a separable function of momentum and guiding-center radius, so that $g_0(r_g,w,u,\phi)=N_0F_0(w,u)G_0(r_g)$ with N_0 the beam density on axis. As a result, Eqs. (9a) and (9b) become

$$\frac{dP(z,t)}{dz}=-\pi N_0 eE_0(z,t)R_b^2H(k_\perp R_b)\int du\int dw\frac{w}{\gamma}F_0(u,w)\times\begin{cases}wJ_m'(k_\perp w/\Omega\gamma)\cos\Delta_m & \text{(10a)}\\ (m\Omega\gamma k_z/k_\perp^2-u)J_m(k_\perp w/\Omega\gamma)\sin\Delta_m, & \text{(10b)}\end{cases}$$

where $\Delta_m=m\phi_0+(mp-\omega)t-(m\xi-k_z)z$, and where $H(k_\perp R_b)$ is a dimensionless beam density form factor given by

$$H(k_\perp R_b)=\frac{2}{R_b^2}\int_0^{R_b}dr_g r_g J_0(k_\perp r_g)G_0(r_g)\ , \tag{11}$$

with R_b the outer guiding-center radius. If the beam is uniform, so that $G_0(r_g)=1$ for $r_g\le R_b$ and zero beyond, one finds that $H(k_\perp R_b)=2J_1(k_\perp R_b)/(k_\perp R_b)$. In the limit of a small spread in guiding centers, such that $k_\perp R_b<1$, one may expand in powers of $k_\perp R_b$ to yield $H(k_\perp R_b)\approx 1-(k_\perp R_b)^2/8+(k_\perp R_b)^4/192-\ldots$. For $k_\perp R_b=1.616$, $H(k_\perp R_b)=0.707$; thus for beams with an outer guiding-center radius larger than about $1.6k_\perp^{-1}$, one can expect the linear growth in wave power [which

will be shown to be proportional to $H^2(k_\perp R_b)$] to be less than half that for a beam with no spread in guiding centers.

We now form a second equation for $dP(z,t)/dz$ from the familiar Poynting relationship

$$P(z,t)=\frac{\pi R^2}{2\eta}\frac{k_z c}{\omega}g_{mn}E_0^2(z,t)\ , \tag{12}$$

where $\eta=(\mu_0/\varepsilon_0)^{1/2}=120\pi$ ohms, $g_{mn}=J_m^2(s'_{mn})(1-m^2/s'^2_{mn})$ for TE_{mn} modes, and $g_{mn}=g'_{mn}=J'^2_m(s_{mn})$ for TM_{mn} modes. If one differentiates Eq. (12) with respect to z and equates the results to Eqs. (10a) and (10b), one finds

$$\frac{dE_0(z,t)}{dz}=-\frac{\eta R_b^2}{R^2}\frac{\omega}{k_z c}\frac{N_0 e}{g_{mn}}H(k_\perp R_b)\int du\int dw\frac{w}{\gamma}F_0(u,w)\begin{cases}wJ'_m(k_\perp w/\Omega\gamma)\cos\Delta_m & \text{(13a)}\\ (m\Omega\gamma k_z/k_\perp^2-u)J_m(k_\perp w/\Omega\gamma)\sin\Delta_m\ . & \text{(13b)}\end{cases}$$

Equations (13a) and (13b) give, for an axisymmetric beam, the instantaneous rates of spatial evolution of the electric-field amplitudes for TE_{mn} and TM_{mn} modes due to interaction with the beam. These rates of change are momentum integrals over oscillatory functions of u, w, z, and t, which, in general, will have small time-averaged values. Moreover, the amplitude $E_0(L)$ will have an oscillatory space dependence with a small cumulative value, after integrating the rates over a finite interaction length L. Only if the argument Δ_m of the trigonometric functions in Eqs. (13a) and (13b) is relatively stationary over the momentum, time, and space intervals of interest is there a possibility for significant time-averaged cumulative growth in the field amplitudes. Below this will be reduced to a quantitative requirement on the frequency difference $(\omega-mp)$ and the momentum-averaged wave-number difference $(k_z-m\bar{\xi})$ necessary for the wave to grow monotonically.

Averaging Eqs. (13a) and (13b) over an interaction time $T=\gamma z/u$ for particles traveling with the wave over an axial distance z, and subsequent integration over z for a total interaction length L to find $E_0(L)$, will involve the integrals

$$I_1(\zeta_1,\zeta_2,m\phi_0)=\frac{u}{\gamma}\int_0^L\frac{dz}{z}\int_0^{\gamma z/u}dt\cos\Delta_m$$
$$=\frac{L}{\zeta_1}\int_{\zeta_2-\zeta_1}^{\zeta_2}\frac{d\zeta}{\zeta}[\sin(m\phi_0+\zeta)-\sin(m\phi_0)] \tag{14a}$$

and

$$I_2(\zeta_1,\zeta_2,m\phi_0)=\frac{u}{\gamma}\int_0^L\frac{dz}{z}\int_0^{\gamma z/u}dt\sin\Delta_m$$
$$=I_1\left[\zeta_1,\zeta_2,m\phi_0+\frac{\pi}{2}\right]\ , \tag{14b}$$

where $\zeta_1=(\omega-mp)\gamma L/u$ and $\zeta_2=(k_z-m\xi)L=[k_z-m\gamma(p-\Omega)/u]L$. The general result for the amplitude of the field is thus

$$E_0(L)-E_0(0)=-\frac{N_0 e\eta\omega R_b^2}{R^2 c k_z g_{mn}}H(k_\perp R_b)\int du\int dw\frac{w}{\gamma}F_0(u,w)\begin{cases}wJ'_m(k_\perp w/\Omega\gamma)I_1(\zeta_1,\zeta_2,m\phi_0) & \text{(15a)}\\ (m\Omega\gamma k_z/k_\perp^2-u)J_m(k_\perp w/\Omega\gamma)I_2(\zeta_1,\zeta_2,m\phi_0), & \text{(15b)}\end{cases}$$

where $E_0(0)$ is the input boundary value of the field. In the following sections of this paper, we will analyze Eqs. (15a) and (15b) to find the linearized power transfer to the wave for a cold beam under conditions of perfect phase matching between the wave and the beam. In addition, we will estimate the effects upon wave growth due to a spread in axial velocities on the beam and due to a phase mismatch. The linear growth of those modes of the waveguide that can compete with a design mode will also be evaluated.

B. Cold-beam limit

For a monoenergetic beam with no spread in pitch angle or guiding-center radius, we have $F_0(u,w)=\delta(u-U)\delta(w-W)/W$ and $H(k_\perp R_b)=1$. Furthermore, an operating point is chosen such that both frequency and wave-number matching occur, e.g.,

$$\omega=mp \tag{16}$$

and

$$k_z=m\xi=m\gamma(p-\Omega)/U\ . \tag{17}$$

In Ref. [1], it is shown that the harmonic coupling coefficient, as given by $K_m=J'_m(k_\perp W/\gamma\Omega)$ for TE modes, will be maximized if

$$\frac{k_\perp W}{\Omega\gamma}=\frac{m\beta_\perp}{(1-\beta_z^2)^{1/2}}=m\left[\frac{\gamma^2\beta_\perp^2}{1+\gamma^2\beta_\perp^2}\right]^{1/2} \tag{18}$$

for $\Omega/p=1-\beta_z^2$, where $\beta_z=U/c\gamma$ and $\beta_\perp=W/c\gamma$. Equations (16)–(18) combine to give $ck_z/\omega=\beta_z$, corresponding to the so-called "grazing condition" wherein the axial velocity of the beam and the group velocity of the wave are equal. Under this condition, it follows that $m\Omega\gamma k_z/k_\perp^2=U$, so that from Eq. (15b) coupling between a cold beam and all TM modes vanishes. This is evidently because, in the net work done by the fields on the beam, an exact cancellation occurs between contributions

from the axial and transverse components. Henceforth in discussing linear theory we will consider only TE modes, since even for operation slightly away from the grazing condition and beams with a spread in pitch angle, power flow into TM modes (while not identically zero) is expected to be much smaller than for TE modes. This supposition is examined in the context of nonlinear theory in Sec. III.

When Eqs. (16) and (17) are satisfied, Eq. (14a) reduces to $I_1(0,0,m\phi_0)=L\cos(m\phi_0)$. In the absence of an external signal $E_0(0)=0$, the relative phase ϕ_0 adjusts itself to maximize the power flow into the wave. Thus

$$E_0(L)=\frac{\eta I_0 L}{\pi R^2\beta_z g_{mn}}\frac{W}{U}K_m \ , \tag{19}$$

and, from Eq. (12)

$$P(L)=\frac{\eta I_0^2 L^2}{2\pi R^2\beta_z g_{mn}}\left[\frac{W}{U}\right]^2 K_m^2 \ , \tag{20}$$

where $I_0=\pi R_b^2 N_0 eU/\gamma$ is the dc beam current. Equations (19) and (20) are similar to results obtained for a cold beam coupling to modes of rectangular waveguides, except for factors to account for the geometric differences. However, other than for a circularly polarized TE_{0m} mode in a square waveguide, there is no selection rule for rectangular waveguides that eliminates coupling to all other modes at the mth harmonic with an axisymmetric beam. This fact mitigates in favor of the use of cylindrical waveguides in devices based on this interaction in order to minimize mode competition problems.

As a conceptual design example, we consider a fifth-harmonic converter for generating power at 94 GHz using a cold 150-kV, 6.667-A beam with $W/U=2.0$. For the TE_{51} waveguide mode, $s'_{51}=6.415\,62$ and $g_{51}=0.0549$. The waveguide radius becomes $R=0.340$ cm, giving $P(L)=20L^2$ kW, for L in cm. This corresponds to a linear efficiency of $2\,L^2\%$. If one assumes that linear theory remains valid up to an efficiency of 10%, these figures indicate that the wave power would reach 100 kW in an interaction length L of 2.24 cm, or about two guide wavelengths. In Sec. IV we will compare this estimate with the exact prediction of nonlinear theory.

The dependence of the fifth-harmonic linear conversion rates at 94 GHz upon beam voltage is shown in Fig. 2, based on Eq. (20). For a beam with $W/U=2.0$, and for operation at the grazing condition for each voltage, Fig. 2 shows the linear normalized power-generation rate $P(L)/L^2I_0^2$, as well as the specific power-generation rate $P(L)/L^2$ for two constant values of beam power, 0.30 and 1.0 MW. As is seen, the normalized power generation rate increases monotonically as voltage increases, but the power generation rate for constant beam power reaches its maximum value at about 115 kV. This fact suggests that an argument to operate a fifth-harmonic converter with a beam having $W/U=2.0$ at beam voltage higher than 115 kV might be based on beam quality considerations for high current beams, but not on conversion efficiency considerations. Figure 2 shows that fifth-harmonic conversion employing a lower voltage beam should be feasible, since the specific power-generation rate does not fall below half the maximum rate unless the beam voltage falls below about 32 kV.

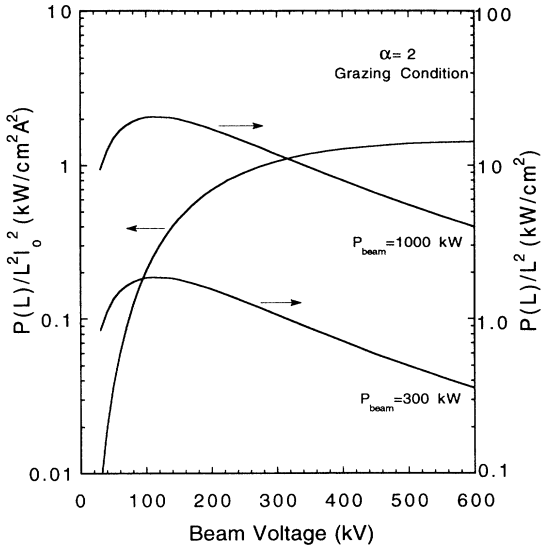

FIG. 2. Predictions of linear theory for normalized fifth-harmonic power-generation rate (left-hand scale) and specific power-generation rate (right-hand scale) for 0.30- and 1.0-MW beams of indicated voltage with $\alpha=2.0$.

C. Diminution in harmonic power generation due to beam velocity spread

Precisely at the harmonics $\omega=mp$, where $\zeta_1=0$, one finds

$$I_1(0,\zeta_2,m\phi_0)=\frac{\sin(m\phi_0+\zeta_2)-\sin(m\phi_0)}{\zeta_2}L \ . \tag{21}$$

Examination of Eq. (15a) indicates that the factor most sensitive to momentum spread is $I_1(0,\zeta_2,m\phi_0)$, due to phase interference between contributions with different values of ζ_2. For a beam with electrons having equal energies but with a spread in pitch angles, as designated by a spread in axial momentum $\Delta u=u_2-u_1$, we estimate the effect on the harmonic power generation rate by evaluating the integral

$$I=\int_{-\infty}^{+\infty}du\,F(u,w)\frac{1}{\zeta_2}[\sin(m\phi_0+\zeta_2)-\sin(m\phi_0)] \ . \tag{22}$$

In order to allow Eq. (22) to be expressed in terms of tabulated functions, we choose the distribution function $F(u,w)=[u_1u_2/u^2\Delta u\,]\delta[w-(c^2\gamma^2-c^2-u^2)^{1/2}]/w$ to characterize a finite spread in u with constant energy. For a narrow spread, such that $\Delta u \ll u_0=(u_1+u_2)/2$, $F(u,w)$ is nearly constant over the interval $u_1<u<u_2$. Changing the variable of integration in Eq. (22) from u to $\zeta_2=k_zL-a/u$, where $a=m\gamma(p-\Omega)L$ allows Eq. (22) to be written as

$$I=\frac{u_1u_2}{a\Delta u}\int_{k_zL-a/u_1}^{k_zL-a/u_2}d\zeta_2\left[\sin(m\phi_0)\left[\frac{\cos\zeta_2-1}{\zeta_2}\right]+\cos(m\phi_0)\left[\frac{\sin\zeta_2}{\zeta_2}\right]\right]. \quad (23)$$

If the harmonic converter is designed to maximize the linear wave growth for a cold beam with axial momentum u_0, then $k_z=m\gamma(p-\Omega)/u_0$ and the limits of integration in Eq. (23) become $\pm\Delta/2$, where $\Delta=k_zL(\Delta u/u_0)$. This leads to

$$I=\frac{2}{\Delta}\left\{\sin(m\phi_0)\left[\mathrm{Ci}\left[\frac{\Delta}{2}\right]-\ln\left[\frac{\Delta}{2}\right]-\gamma_E\right]+\cos(m\phi_0)\left[\mathrm{Si}\left[\frac{\Delta}{2}\right]\right]\right\}, \quad (24)$$

where $\mathrm{Si}(x)$ and $\mathrm{Ci}(x)$ are the sine-integral and cosine-integral functions [19], and where $\gamma_E=0.577\,216$ is Euler's constant. The relative phase angle ϕ_0 between the field and the current will adjust itself to maximize the rate of power transfer from the beam to the fields. For a function as is given in Eq. (24) of the form $f(\phi_0)=A\sin(m\phi_0)+B\cos(m\phi_0)$ the maximum value, found by differentiation with respect to $m\phi_0$, is $f^2_{\max}=A^2+B^2$. This gives the value of $I_{\max}$ corresponding to maximum power transfer to the fields to be

$$I^2_{\max}=\frac{4}{\Delta^2}\left\{\left[\mathrm{Ci}\left[\frac{\Delta}{2}\right]-\ln\left[\frac{\Delta}{2}\right]-\gamma_E\right]^2+\left[\mathrm{Si}\left[\frac{\Delta}{2}\right]\right]^2\right\}. \quad (25)$$

Figure 3 is a plot of $I^2_{\max}$ as a function of Δ in the range of $0<\Delta<20$. Since the power growth from linearized theory in the absence of an input field $E_0(0)$ is proportional to $I^2_{\max}$, one sees from Fig. 3 that the growth would fall to half its value for a corresponding cold beam if $\Delta=7.65$. This corresponds to $\Delta u/u_0=7.65/k_zL$, which is roughly equivalent to the condition $\Delta u/u_0=N^{-1}$, where N is the number of interaction guide wavelengths in the harmonic converter. Similarly, one sees from Fig. 3 that the power growth will not be less than 90% its value for a cold beam if $\Delta<2.90$, corresponding to $\Delta u/u_0<0.48N^{-1}$. Such conditions for the diminution of growth are not uncommon for traveling-wave interactions, such as in free-electron lasers in the low gain limit [20].

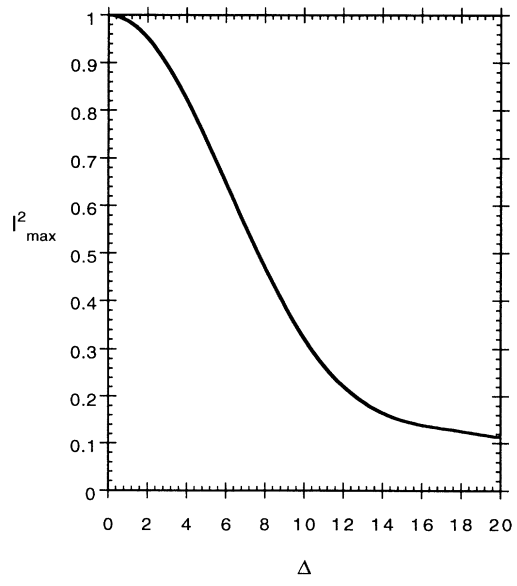

FIG. 3. Diminution in linearized power generation rate as a function of axial momentum spread $\Delta=k_zL(\Delta u/u_0)$, as predicted by Eq. (25).

D. Power growth in competing modes

This section presents an estimate of the rate of power flow into TE modes other than the design mode. The system parameters are chosen to optimize the linear rate of power transfer to the design mode, so that matching between the group velocity of the wave and the axial velocity of the beam will, in general, not occur for the competing modes. In addition, it will be shown that parameters may be chosen so that radiation at harmonics lower than the design harmonic is cut off in those waveguide modes at which power growth is not already prohibited by the selection rule discussed with regard to Eqs. (9a) and (9b).

For a cold axisymmetric beam, and for power growth at the harmonics $\omega=mp$, the value of relative phase $m\phi_0$ between the current and the electric field that leads to maximum growth rate for the field can be found from Eq. (21) to be $\pi-\zeta_2/2$. At this relative phase, $I_1(0,\zeta_2,\pi-\zeta_2/2)=-(\sin\delta/\delta)L$, where $\delta=(k_{zc}-m_ck_{zd}/m_d)L/2$, with k_{zc} and m_c the wave number and harmonic number for the competing mode and k_{zd} and m_d those for the design mode. As a result, we can find the power in a competing mode $P_c(L)$ from Eq. (20) to be

$$P_c(L)=P_d(L)\frac{k_{zd}}{k_{zc}}\frac{g_{mnd}}{g_{mnc}}\frac{m_c}{m_d}\left[\frac{K_{mc}}{K_{md}}\right]^2\left[\frac{\sin\delta}{\delta}\right]^2, \quad (26)$$

where $P_d(L)$ is the power in the design mode, K_{md} and K_{mc} are the harmonic coupling coefficients for the design mode and a competing mode, and g_{mnd} and g_{mnc} are the geometric scaling factors [see Eq. (12)] for the design mode and a competing mode. Equation (26) shows that power in a competing mode will not grow cumulatively with interaction length L due to phase mismatch with the beam, as embodied in the factor $(\sin\delta/\delta)^2$.

Of course, since Eq. (26) is based on linearized theory, it assumes that the design mode and any competing modes grow independently of one another. Clearly this is not the case when the individual mode powers become significant, and competing modes can be expected to influence the beam distribution and thus one another's growth. Nonlinear mode competing is illustrated and discussed in Sec. III.

To illustrate the influence of the aforementioned phase mismatch on the linearized growth of competing modes, we consider for the design mode a fifth-harmonic con-

verter discussed in Sec. II B, the parameters for which are listed in Table I. The growth of harmonic power at competing harmonics m for the device parameters given in Table I has been calculated from Eq. (26) for harmonics up to the eighth. Except for the TE_{41} mode, all TE modes at harmonics below the design harmonic $m=5$ are cut off. Table II gives relevant parameters and the four most serious competing modes TE_{41}, TE_{61}, TE_{71}, and TE_{81} at $m=4$, 6, 7, and 8, respectively.

Table II shows that the harmonic coupling coefficient K_m decreases with harmonic number by an order of magnitude between $m=4$ and 8. The initial growth rate $P(L)/L^2$ for $m=4$ exceeds that for $m=5$ by a factor of 12, but the growth rates for $m=6$, 7, and 8 are successively smaller than that for $m=5$. However, after an interaction length L of 5 cm, the $m=4$ and 6 modes have grown to only 4.7% and 1.2% of the $m=5$ mode due to phase mismatch. While these predictions are based on linearized theory, which is neither competent to treat the mutual interaction of several modes, nor indeed the (clearly nonlinear) growth of the $m=5$ mode to 500 kW, the results suggest strongly that the powerful effect of phase mismatch can be highly effective in suppressing potentially competitive modes.

In the above example, it was noted that the harmonics $m=1$, 2, and 3 did not interact with the beam because the TE_{11}, TE_{21}, and TE_{31} modes are all cut off at the corresponding harmonic frequencies. One can derive a condition that would insure that all harmonics lower than the design harmonic be cut off for TE_{ml} modes of a cylindrical waveguide. This condition is simply

$$(1-\beta_z^2)^{1/2} > \frac{m-1}{m}\frac{f_m}{f_{m-1}}, \tag{27}$$

where m is the harmonic number for the design mode, and f_m and f_{m-1} are cutoff frequencies for the waveguide in the design mode and in the next lower TE_{m1} mode. For the example above, with $m=5$ as the design mode, this condition gives $\beta_z < 0.2615$, corresponding to $\alpha > 2.21$ for a beam voltage of 150 kV. Table III gives the maximum values of β_z that satisfy Eq. (27) for $2 \le m \le 10$, together with the respective maximum values of velocity ratio $\alpha = W/U$ that these figures imply. Such considerations indicate that it is possible to suppress coupling to all harmonics lower than the design harmonic by use of a beam with sufficiently high velocity ratio.

TABLE I. Parameters for conceptual design device to generate fifth-harmonic power at 94-GHz. These parameters are used in calculating the growth of competing models in Table II.

Frequency $\omega/2\pi$	94.0 GHz
Waveguide radius R	0.3398 cm
Waveguide design mode	TE_{51}
Beam voltage	150 kV
Beam current I_0	6.667 A
Velocity ratio $\alpha = W/U$	2.0
Magnetic field B	7.983 kG
Power growth rate $P(L)/L^2$	20.05 kW/cm^2

III. SLOW-TIME-SCALE FORMULATION OF NONLINEAR DYNAMICS

Since the linear theory for harmonic conversion given above shows that modes at undesired harmonics could compete with the design mode, a multimode nonlinear analysis is needed to determine efficiency limits and mode purity. The analysis to be presented here is based on a three-dimensional slow-time-scale formulation [21–24] developed for steady-state operation of gyrotrons traveling-wave amplifiers. In this formulation, the electromagnetic field is expanded as a superposition of unperturbed TE and TM modes of an empty waveguide. Maxwell's equations are averaged over a wave period, allowing a series of slow-time-scale equations to be derived for the evolution of the amplitude and phase of each TE and TM mode as driven by an electron beam in an external guide magnetic field. In general, the guide magnetic field is axisymmetric but nonuniform. The modes are coupled through their mutual nonlinear interaction with the ensemble of beam electrons. The wave-period averaging allows multimode interactions to be considered provided the frequencies are integral multiples of a fundamental frequency, and provided the time average is done over the fundamental wave period. In this case, the particles that enter the interaction region at times separated by integral multiples of the fundamental wave period will execute identical trajectories even though they interact with many modes. The time-averaged field equations are integrated simultaneously with the three-dimensional Lorentz force equations that determine the particle orbits. No averaging is done for the orbit equations. The trajectory of each particle is calculated by summing con-

TABLE II. Parameters at harmonics up to $m=8$ for modes that can compete with the fifth-harmonic design mode TE_{51}, based on linearized theory. The cutoff frequencies are given under the column headed f_m.

m	mode	f (GHz)	f_m (GHz)	k_z (cm^{-1})	K_m	$P(L)/L^2$ (kW/cm^2)	P ($L=1$ cm) (kW)	P ($L=5$ cm) (kW)
4	TE_{41}	75.20	74.72	1.779	0.1299	248.2	130.8	23.6
5	TE_{51}	94.00	90.15	5.578	0.0616	20.0	20.1	500.1
6	TE_{61}	112.80	105.40	8.414	0.0354	5.1	4.4	5.8
7	TE_{71}	131.60	120.53	11.065	0.0212	1.6	0.6	0.56
8	TE_{81}	150.40	135.56	13.644	0.0130	0.6	0.005	0.005

TABLE III. Maximum β_z values for suppression of coupling to TE_{m1} modes at all harmonics below the design harmonic for harmonics from 2 to 10. Also shown are the corresponding values for the minimum velocity ratio $\alpha_{\min}$ for several beam voltages, including the limit of infinite beam voltage. The asymptotic value of $\beta_{z\,\max}$ for large m is $1.038\,34m^{-5/6}$.

Design harmonic number m	$\beta_{z\,\max}$	$\alpha_{\min}$ 150 kV	500 kV	1 MV	5 MV	∞
2	0.558 63	0.5379	1.1772	1.3557	1.4754	1.4847
3	0.398 84	1.2367	1.9184	2.1372	2.2874	2.2992
4	0.314 40	1.7523	2.5558	2.8213	3.0049	3.0194
5	0.261 51	2.2099	3.1444	3.4569	3.6738	3.6909
6	0.225 04	2.6353	3.7016	4.0605	4.3100	4.3297
7	0.198 21	3.0400	4.2369	4.6414	4.9229	4.9451
8	0.177 62	3.4283	4.7539	5.2031	5.5158	5.5405
9	0.161 33	3.8025	5.2541	5.7469	6.0902	6.1173
10	0.147 76	4.1748	5.7534	6.2900	6.6640	6.6934

tributions from each mode. The nonlinear single-mode equations for gyrotron traveling-wave amplifiers including the effects of guiding-center motion, axial electron velocity spread, and nonuniform guide field have been derived for TE modes in rectangular electrodynamic structures [21,22] and in cylindrical geometry. The theory is extended here to multimode interactions with both TE and TM modes.

The self-consistent evolution of the electromagnetic field and the trajectories of an ensemble of electrons are determined by solving Maxwell's wave equation and the Lorentz force equation simultaneously, e.g.,

$$\nabla^2\mathbf{E}-\mu_0\varepsilon_0\frac{\partial^2\mathbf{E}}{\partial t^2}=\mu_0\frac{\partial\mathbf{J}}{\partial t}\ , \tag{28}$$

$$\frac{d}{dt}(\gamma\mathbf{v})=-\frac{e}{m_0}(\mathbf{E}+\mathbf{v}\times[\mathbf{B}_0+\mathbf{B}])\ , \tag{29}$$

where $\mathbf{B}_0$ is the axial guide magnetic field, and $\mathbf{E}$ and $\mathbf{B}$ are the rf electric and magnetic fields, respectively. The electron velocity is $\mathbf{v}$ and the current density is $\mathbf{J}$. The relativistic factor $\gamma^2=(1-\mathbf{v}\cdot\mathbf{v}/c^2)^{-1}=1+(w^2+u^2)/c^2$. We will hereafter use $v_z=u/\gamma$ and $v_\perp=w/\gamma$, the magnitudes of the axial and transverse components of the velocity of the electron. The guide magnetic field $\mathbf{B}_0(z)$ may be weakly nonuniform but axisymmetric. Thus we write

$$\mathbf{B}_0(\mathbf{r})\approx B_0(z)\hat{\mathbf{e}}_z-\frac{1}{2}\frac{\partial B_0}{\partial z}r\hat{\mathbf{e}}_r\ .$$

The source current may be expressed [12] as

$$\mathbf{J}(\mathbf{r},z,t)=-\frac{I_0}{\langle v_{z0}\rangle}\int\int\int d^3v\int\int d^2r_0\int_0^T dt_0 f_0(\mathbf{v},\mathbf{r}_0,t_0)v_z(0)\frac{\mathbf{v}'(\mathbf{r}',z,t')}{|v_z(\mathbf{r}_0,z,t_0)|}\delta(\mathbf{r}'-\mathbf{r}(\mathbf{r}_0,z,t_0))\delta(t'-\tau(\mathbf{r}_0,z,t))\ , \tag{30}$$

where the dc current $I_0=en_b\langle v_{z0}\rangle A_b$, with n_b the average electron density, A_b the cross-sectional area of the beam and $\langle v_{z0}\rangle$ the average velocity of the electrons at $z=0$, the entrance to the interaction region. The vector $\mathbf{r}$ denotes the transverse position of an electron. The quantities at $z=0$ are denoted by a subscript "0"; $\mathbf{v}(z,\mathbf{r}_0,t_0)$ is the velocity of an electron which crossed the $z=0$ plane at time t_0 in the transverse position $\mathbf{r}_0$, and T is the interaction time. The system is assumed to be time periodic, so that $\mathbf{v}(z,\mathbf{r}_0,t_0)=\mathbf{v}(z,\mathbf{r}_0,t_0+2\pi j/\omega_0)$, where j is an integer. The time interval τ is defined by

$$\tau(z,\mathbf{r}_0,t_0)=t_0+\int_0^z dz'[v_z(z',\mathbf{r}_0,t_0)]^{-1}\ .$$

The initial distribution function of the electrons in cross section, time and velocity is denoted by $f_0(\mathbf{v},\mathbf{r}_0,t_0)$ subject to the normalization

$$\frac{1}{T}\int_0^T dt_0\int\int\int d^3v\int\int d^2r_0 f_0(\mathbf{v},\mathbf{r}_0,t_0)=1\ .$$

In the absence of an input signal, the solution of Eq. (29) in a uniform field $\mathbf{B}_0$ represents Larmor rotation around a guiding center that drifts along the axis with velocity v_z. The gyration frequency is $\Omega=eB_0/\gamma m_0$, and the gyration radius $r_L=v_\perp/\Omega$. When $\mathbf{E}$ and $\mathbf{B}$ are nonzero and $\mathbf{B}_0$ is weakly nonuniform, the electron trajectories can still be described as a superposition of the guiding-center motion and a Larmor precession about the guiding center (see Fig. 1) where v_z, $v_\perp$, Ω, r_L, and the guiding-center coordinates (r_g,θ_g) vary slowly in space. Thus

$$\begin{aligned}\mathbf{r}&=(r_g\cos\theta_g+r_L\cos\phi)\hat{\mathbf{e}}_x+(r_g\sin\theta_g+r_L\sin\phi)\hat{\mathbf{e}}_y+z\hat{\mathbf{e}}_z\\&=r\hat{\mathbf{e}}_r+z\hat{\mathbf{e}}_z\ ,\end{aligned} \tag{31}$$

where $r^2=r_g^2+r_L^2+2r_gr_L\cos(\phi-\theta_g)$, and

$$\begin{aligned}\frac{d\mathbf{r}}{dt}=\mathbf{v}&=-(v_\perp\sin\phi)\hat{\mathbf{e}}_x+(v_\perp\cos\phi)\hat{\mathbf{e}}_y+v_z\hat{\mathbf{e}}_z\\&=-v_\perp\sin(\phi-\theta)\hat{\mathbf{e}}_r+v_\perp\cos(\phi-\theta)\hat{\mathbf{e}}_\theta+v_z\hat{\mathbf{e}}_z\ ,\end{aligned} \tag{32}$$

where $v_\perp = r_L\Omega(z) = r_L\Omega_0(z)/\gamma(z)$. The gyration phase ϕ reduces to Ωt in the limit $\mathbf{E}=\mathbf{B}=\mathbf{0}$. Equations (31) and (32) imply that the guiding-center motion in the transverse plane is determined by

$$\frac{dr_g}{dt}+\frac{dr_L}{dt}\cos(\phi-\theta_g)-r_L\left[\frac{d\phi}{dt}-\Omega\right]\sin(\phi-\theta_g)=0\ , \tag{33}$$

$$r_g\frac{d\theta_g}{dt}+\frac{dr_L}{dt}\sin(\phi-\theta_g)-r_L\left[\frac{d\phi}{dt}-\Omega\right]\cos(\phi-\theta_g)=0\ , \tag{34}$$

It will be convenient to use a complex notation for $\mathbf{v}$, $\mathbf{E}$, and $\mathbf{B}$ and take real parts. Hence, we write Eq. (32) in the form

$$\mathbf{v}=\mathrm{Re}(i\hat{\mathbf{e}}_r+\hat{\mathbf{e}}_\theta)v_\perp\exp[i(\phi-\theta)]+v_z\hat{\mathbf{e}}_z\ , \tag{35}$$

where Re denotes the real part.

Similarly, in the absence of a source current ($\mathbf{J}=\mathbf{0}$), the solutions to Eq. (28) form a complete set of orthogonal basis functions comprising the TE and TM modes of the vacuum waveguide where the amplitude and axial wave vector are constants. In the presence of a tenuous beam, we may expand $\mathbf{E}$ and $\mathbf{B}$ in terms of this compete set of basis functions and assume that the amplitude and axial wave vector vary slowly in space. Thus we write

$$\mathbf{E}(\mathbf{r},t)=\frac{m_0c^2}{eR}\sum_{q=1,2}\sum_{\substack{n=1\\m=0}}^{\infty}A_{mn}^{(q)}(z)\mathbf{e}_{mn}^{(q)}(r,\theta)\exp\left[i\left[\omega_{mn}^{(q)}t-\int_0^z dz'k_{z,mn}^{(q)}(z')\right]\right]\ , \tag{36}$$

where the superscript q represents TE ($q=1$) and TM ($q=2$) modes, respectively. The wave amplitude $A_{mn}^{(q)}(z)$ and the axial wave vector $k_{z,mn}^{(q)}(z)$ vary slowly along the axis of the waveguide. The angular frequency of the mode ω_{mn} must be an integral multiple of a fundamental frequency ω_0. The set of basis functions $\mathbf{e}_{mn}^{(q)}(r,\theta)$ for TE and TM modes are given by

$$\mathbf{e}_{mn}^{(1)}(r,\theta)=C'_{mn}s'_{mn}\left[\frac{imJ_m(k'_{mn}r)}{k'_{mn}r}\hat{\mathbf{e}}_r+J'_m(k'_{mn}r)\hat{\mathbf{e}}_\theta\right]e^{-im\theta} \tag{37}$$

and

$$\mathbf{e}_{mn}^{(2)}(r,\theta)=C_{mn}s_{mn}\left[J'_m(k_{mn}r)\hat{\mathbf{e}}_r-\frac{imJ_m(k_{mn}r)}{k_{mn}r}\hat{\mathbf{e}}_\theta+\frac{ik_{mn}}{k_{zmn}}J_m(k_{mn}r)\hat{\mathbf{e}}_z\right]e^{-im\theta}\ , \tag{38}$$

where for TE modes $k'_{mn}R=s'_{mn}$, the nth zero of $J'_m(s)$; and for TM modes $k_{mn}R=s_{mn}$, the nth zero of $J_m(s)$. Equations (37) and (38) satisfy the customary boundary conditions at the perfectly conducting waveguide wall, namely the vanishing of tangential $\mathbf{E}$ and normal $\mathbf{B}$. The coefficients C_{mn} are given for TM modes by

$$C_{mn}^{-1}=\sqrt{\pi}s_{mn}J'_m(s_{mn})=s_{mn}(\pi g_{mn})^{1/2} \tag{39}$$

and for TE modes by

$$C'^{-1}_{mn}=\sqrt{\pi}(s'^2_{mn}-m^2)^{1/2}J_m(s'_{mn})=s'_{mn}(\pi g'_{mn})^{1/2}\ . \tag{40}$$

The basis functions as given in Eqs. (37) and (38) are for right-hand circularly polarized waves. It is convenient to introduce a normalization scheme in which the waveguide radius R is scaled out of the equations. The appropriate normalized variables are defined as follows:

$$\zeta=z/R,\quad \rho=r/R,\quad \chi_{mn}=k_{zmn}R\ ,$$
$$\bar{\omega}=\omega R/c,\quad \beta_z=v_z/c,\quad \beta_\perp=v_\perp/c\ ;$$
$$\bar{E}=\frac{eR}{mc^2}E,\quad \bar{B}=\frac{eR}{mc}B\ .$$

From Maxwell's equation $\nabla\times\mathbf{E}=-\partial\mathbf{B}/\partial t$, the magnetic-field components may be expressed as

$$B_r(r,\theta,z,t)=-\mathrm{Re}\sum_{q=1}^{2}\sum_{m,n}\frac{\hat{k}_{mn}^{(q)}}{c\bar{\omega}_{mn}}E_{\theta,mn}^{(q)}\ , \tag{41}$$

$$B_\theta(r,\theta,z,t)=-\mathrm{Re}\sum_{q=1}^{2}\sum_{m,n}\frac{\hat{k}_{m,n}^{(q)}}{c\bar{\omega}_{mn}}E_{r,mn}^{(q)}\ , \tag{42}$$

$$B_z(r,\theta,z,t)=-\mathrm{Re}\sum_{m,n}\frac{s'^2_{m,n}\rho}{c\bar{\omega}_{mn}m}E_{r,mn}^{(1)}\ , \tag{43}$$

where the normalized wave numbers are

$$\hat{k}_{mn}^{(1)}=\chi_{mn}^{(1)}+i\Gamma_{mn}^{(1)}\ ,$$
$$\hat{k}_{mn}^{(2)}=\chi_{mn}^{(2)}\left\{1+\left[\frac{s_{mn}}{\chi_{mn}^{(2)}}\right]^2\right\}+i\Gamma_{mn}^{(2)}\ ,$$

with the normalized growth rate

$$\Gamma_{mn}^{(q)}=\frac{1}{A_{mn}^{(q)}}\frac{dA_{mn}^{(q)}}{d\zeta}\ . \tag{44}$$

For clarity, the superscript "q" will be suppressed unless required to avoid ambiguity. Substitution of the fields [Eqs. (36)–(43)] and the source current [Eqs. (30) and (35)] in Eq. (28) leads to the dynamical equations which govern the evolution of the slowly varying amplitude $A_{mn}^{(q)}$ and axial wave vector $\chi_{mn}^{(q)}$ of each mode. These equations are obtained by taking the scalar product of $\mathbf{E}$ with the terms on both sides of Eq. (28), averaging over a fundamental wave period $T=2\pi/\omega_0$ and integrating over the cross section of the waveguide, using the orthogonality properties of the basis functions. The

resulting expressions involve Bessel functions with argument $k_{mn}r$ or $k'_{mn}r$. Since r is given by Eq. (31), Graff's addition theorem [18] can be used to expand the Bessel functions in an infinite series of cyclotron harmonics, with phases for the terms in the expansion varying as $\exp(i\varphi_{mn})$, where

$$\varphi_{mn}=\omega_{mn}t-s\phi-(m-s)\theta_g-\int_0^z dz' k_{z,mn}(z') \ . \tag{45}$$

The harmonic number s ranges from $-\infty$ to $+\infty$. From the infinite series, we will retain a single sth cyclotron harmonic for which the beam mode and the guide mode are close to resonance and for which the phase detuning parameter φ_{mn} varies slowly in time. The phase detuning for all other harmonics will vary rapidly with time and the time-averaged contribution of the terms will tend to vanish, as discussed in Sec. II A.

After some lengthy algebra, the dispersion of each TE mode in the presence of the electron beam is found to be

$$\frac{d^2A_{mn}}{d\xi^2}+(\bar{\omega}_{mn}^2-s_{mn}'^2-\chi_{mn}^2)A_{mn} =-2\frac{I_0}{I_A}\bar{\omega}_{mn}C'_{mn}s'_{mn} \times\left\langle\frac{\beta_{z0}}{\langle\beta_{z0}\rangle}\frac{\beta_\perp}{|\beta_z|}Q'_{mn}\sin(\varphi_{mn})\right\rangle' \tag{46}$$

and the amplification of the mode is given by

$$\frac{d}{d\xi}(\chi_{mn}A_{mn}^2)=2\frac{I_0}{I_A}\bar{\omega}_{mn}A_{mn}C'_{mn}s'_{mn} \times\left\langle\frac{\beta_{z0}}{\langle\beta_{z0}\rangle}\frac{\beta_\perp}{|\beta_z|}Q'_{mn}\cos(\varphi_{mn})\right\rangle \ , \tag{47}$$

where

$$\begin{aligned} I_A&=\varepsilon_0 m_0 c^3/e \ , \\ Q'_{mn}&=J_{m-s}(s'_{mn}\rho_g)J'_s(s'_{mn}\rho_L) \ , \\ \rho_g&=r_g/R \ , \\ \rho_L&=r_L/R \ . \end{aligned} \tag{48}$$

The angular brackets in Eqs. (46) and (47) denote an average over the initial phase space distribution of the electrons.

Similarly, we find that the evolution of the TM modes is governed by

$$\frac{d^2A_{mn}}{d\xi^2}+(\bar{\omega}_{mn}^2-s_{mn}^2-\chi_{mn}^2)\left[1+\frac{s_{mn}^2}{\chi_{mn}^2}\right]A_{mn}=2\frac{I_0}{I_A}\bar{\omega}_{mn}C_{mn}s_{mn}\left\langle\frac{\beta_{z0}}{\langle\beta_{z0}\rangle}\frac{\beta_\perp}{|\beta_z|}H_{mn}\left[1-\frac{s_{mn}^2\rho_L\beta_z}{s\beta_\perp\chi_{mn}}\right]\cos(\varphi_{mn})\right\rangle \ , \tag{49}$$

$$\frac{d}{d\xi^2}\left[\chi_{mn}\left[1+\frac{s_{mn}^2}{\chi_{mn}^2}\right]A_{mn}^2\right]=2\frac{I_0}{I_A}\bar{\omega}_{mn}A_{mn}C_{mn}s_{mn}\left\langle\frac{\beta_{z0}}{\langle\beta_{z0}\rangle}\frac{\beta_\perp}{|\beta_z|}H_{mn}\left[1-\frac{s_{mn}^2\rho_L\beta_z}{s\beta_\perp\chi_{mn}}\right]\sin(\varphi_{mn})\right\rangle \ , \tag{50}$$

where

$$H_{mn}=J_{m-s}(s_{mn}\rho_g)\frac{sJ_s(s_{mn}\rho_L)}{s_{mn}\rho_L} \ . \tag{51}$$

The two terms in the factor

$$\left[1-\frac{s_{mn}^2\rho_L\beta_z}{s\beta_\perp\chi_{mn}}\right]$$

that arise from $\mathbf{J}_\perp\cdot\mathbf{E}_\perp$ and J_zE_z are of opposite sign. When the wave group velocity $k_{z,mn}c^2/\omega_{mn}$ equals the axial beam velocity v_z, the two terms cancel one another. For a cold beam this indicates that the TM mode interaction does not affect the wave dispersion or growth, as was shown in the linear analysis of Eq. (15b).

The electron orbit equations in the presence of the static and rf fields have to be calculated by summing the contributions for each mode, where the mode coupling arises through the orbit equations. On substitution of the superposition of fields from all TE and TM modes in the complete Lorentz force equation, we obtain the slow-time-scale orbit equations after applying Graff's theorem and keeping a single cyclotron harmonic with resonant phase as described above. For spatial growth of a steady-state excitation, it is convenient to integrate the equations of motion in z rather that t using the relation along electron trajectories.

$$\frac{d\tau}{d\xi}=\frac{1}{\beta_z} \ , \tag{52}$$

where the normalized time is defined by $\tau=ct/R$.

The variations of electron momentum and phase are given by

$$\frac{d(\gamma\beta_\perp)}{d\zeta}=\frac{1}{2}\frac{\partial\bar{\Omega}_0}{\partial\zeta}\rho_L-\sum_{\text{TE modes}}\frac{\hat{A}_{mn}}{\beta_z}Q'_{mn}\left[\left[1-\frac{\beta_z\chi_{mn}}{\bar{\omega}_{mn}}\right]\cos(\varphi_{mn})+\frac{\Gamma\beta_z}{\bar{\omega}_{mn}}\sin(\varphi_{mn})\right]$$
$$-\sum_{\text{TM modes}}\frac{\hat{A}_{mn}}{\beta_z}H_{mn}\left[\left[1-\frac{\beta_z(\chi_{mn}+s_{mn}^2/\chi_{mn})}{\bar{\omega}_{mn}}\right]\sin(\varphi_{mn})-\frac{\Gamma\beta_z}{\bar{\omega}_{mn}}\cos(\varphi_{mn})\right], \tag{53}$$

$$\frac{d(\gamma\beta_z)}{d\zeta}=-\frac{1}{2}\frac{\partial\bar{\Omega}_0}{\partial\zeta}\alpha\rho_L-\sum_{\text{TE modes}}\frac{\hat{A}_{mn}\alpha}{\bar{\omega}_{mn}}Q'_{mn}[\chi_{mn}\cos(\varphi_{mn})-\Gamma\sin(\varphi_{mn})]$$
$$-\sum_{\text{TM modes}}\frac{\hat{A}_{mn}\alpha}{\bar{\omega}_{mn}}H_{mn}\left\{\left[\chi_{mn}+\frac{s_{mn}^2}{\chi_{mn}}\left[1-\frac{\rho_L\bar{\omega}_{mn}}{s\beta_\perp}\right]\right]\sin(\varphi_{mn})+\Gamma\cos(\varphi_{mn})\right\}, \tag{54}$$

$$\frac{d\phi}{d\zeta}=\frac{\bar{\Omega}_0}{\gamma\beta_z}-\sum_{\text{TE modes}}\frac{\hat{A}_{mn}H'_{mn}}{\gamma\beta_z\beta_\perp}\left[\left[1-\frac{\beta_z\chi_{mn}}{\bar{\omega}_{mn}}-\frac{s'^2_{mn}\rho_L^2\bar{\Omega}_0}{s\gamma\bar{\omega}_{mn}}\right]\sin(\varphi_{mn})-\frac{\Gamma\beta_z}{\bar{\omega}_{mn}}\cos(\varphi_{mn})\right]$$
$$+\sum_{\text{TM modes}}\frac{\hat{A}_{mn}Q_{mn}}{\gamma\beta_z\beta_\perp}\left\{\left[1-\frac{\beta_z}{\bar{\omega}_{mn}}\left[\chi_{mn}+\frac{s_{mn}^2}{\chi_{mn}}\right]\right]\cos(\varphi_{mn})+\frac{\Gamma\beta_z}{\bar{\omega}_{mn}}\sin(\varphi_{mn})\right\}, \tag{55}$$

where $\hat{A}_{mn}=C'_{mn}s'_{mn}A_{mn}$ for TE modes, $\hat{A}_{mn}=C_{mn}s_{mn}A_{mn}$ for TM modes, $\bar{\Omega}_0=\Omega_0R/c$, and $\alpha=v_\perp/v_z$. In Eq. (55) Q_{mn} is given by Eq. (48) with s_{mn} in place of s'_{mn}, while H'_{mn} is given by Eq. (51) with s'_{mn} in place of s_{mn}. The rate of change of energy of an electron can be calculated from Eqs. (53) and (54):

$$\frac{d\gamma}{d\zeta}=-\sum_{\text{TE modes}}\hat{A}_{mn}Q'_{mn}\alpha\cos(\varphi_{mn})-\sum_{\text{TM modes}}\hat{A}_{mn}H_{mn}\alpha\left[1-\frac{s_{mn}^2\rho_L\beta_z}{s\beta_\perp\chi_{mn}}\right]\sin(\varphi_{mn}). \tag{56}$$

Equation (56) also shows that the interaction with TM modes vanishes at grazing incidence.

$$\frac{d\rho_g}{d\zeta}=-\frac{1}{2\bar{\Omega}_0}\frac{\partial\bar{\Omega}_0}{\partial\zeta}\rho_g+\sum_{\text{TE modes}}\frac{\hat{A}_{mn}N_{mn}}{\beta_z\bar{\Omega}_0}\left[\left[1-\frac{\beta_z\chi_{mn}}{\bar{\omega}}-\frac{s\bar{\Omega}_0}{\gamma\bar{\omega}}+\frac{M'_{mn}}{N_{mn}}\frac{s'_{mn}\rho_L\bar{\Omega}_0}{\gamma\bar{\omega}}\right]\cos(\varphi_{mn})+\frac{\Gamma\beta_z}{\bar{\omega}}\sin(\varphi_{mn})\right]$$
$$+\sum_{\text{TM modes}}\frac{\hat{A}_{mn}M_{mn}}{\beta_z\bar{\Omega}_0}\left\{\left[1-\frac{\beta_z}{\bar{\omega}}\left[\chi_{mn}+\frac{s_{mn}^2}{\chi_{mn}}\right]\right]\sin(\varphi_{mn})-\frac{\Gamma\beta_z}{\bar{\omega}}\cos(\varphi_{mn})\right\}, \tag{57}$$

$$\rho_g\frac{d\theta_g}{d\zeta}=\sum_{\text{TE modes}}\frac{\hat{A}_{mn}M_{mn}}{\beta_z\bar{\Omega}_0}\left[\left[1-\frac{\beta_z\chi_{mn}}{\bar{\omega}}-\frac{s\bar{\Omega}_0}{\gamma\bar{\omega}}+\frac{N'_{mn}}{M_{mn}}\frac{s'_{mn}\rho_L\bar{\Omega}_0}{\gamma\bar{\omega}}\right]\sin(\varphi_{mn})-\frac{\Gamma\beta_z}{\bar{\omega}}\cos(\varphi_{mn})\right]$$
$$-\sum_{\text{TM modes}}\frac{\hat{A}_{mn}N_{mn}}{\beta_z\bar{\Omega}_0}\left\{\left[1-\frac{\beta_z}{\bar{\omega}}\left[\chi_{mn}+\frac{s_{mn}^2}{\chi_{mn}}\right]\right]\cos(\varphi_{mn})+\frac{\Gamma\beta_z}{\bar{\omega}}\sin(\varphi_{mn})\right\}, \tag{58}$$

where for TE modes

$$N_{mn}=J'_{m-s}(s'_{mn}\rho_g)J_s(s'_{mn}\rho_L),$$
$$M_{mn}=\frac{(m-s)J_{m-s}(s'_{mn}\rho_g)J_s(s'_{mn}\rho_L)}{s'_{mn}\rho_g},$$
$$N'_{mn}=J'_{m-s}(s'_{mn}\rho_g)J'_s(s'_{mn}\rho_L), \tag{59}$$
$$M'_{mn}=\frac{(m-s)J_{m-s}(s_{mn}\rho_g)J'_s(s'_{mn}\rho_L)}{s'_{mn}\rho_g}.$$

For TM modes, the eigenvalues s_{mn} appear in place of s'_{mn} in N_{mn}, N'_{mn}, M_{mn}, and M'_{mn}.

The total transmitted power in the circuit from all TE and TM modes is calculated from the Poynting flux. The time-averaged power flow is given by

$$P=\tfrac{1}{2}\mathrm{Re}\int_0^R dr\,r\int_0^{2\pi}d\theta(\mathbf{E}\times\mathbf{H})\cdot\hat{\mathbf{e}}_z$$
$$=\frac{\varepsilon_0m_0^2c^5}{2e}\left[\sum_{\text{TE modes}}\frac{\chi_{mn}}{\bar{\omega}_{mn}}A_{mn}^{(1)^2}+\sum_{\text{TM modes}}\frac{\chi_{mn}}{\bar{\omega}_{mn}}\left[1+\frac{s_{mn}^2}{\chi_{mn}^2}\right]A_{mn}^{(2)^2}\right]. \tag{60}$$

The nonlinear equations for the fields [Eqs. (46)–(51)] and the electron orbits [Eqs. (52)–(58)] apply to arbitrary values of the guiding-center radius and the Larmor radius. We have included a single cyclotron harmonic at each frequency in the multimode formulation. The theory can be easily adapted to treat the excitation of multiple cyclotron harmonics at a given frequency by including appropriate number of terms from Graff's addition theorem in the field and orbit equations.

IV. NUMERICAL RESULTS

The set of coupled field and orbit equations derived in Sec. III is numerically integrated in z employing a modified version of the fourth-order Runge-Kutta algorithm (Gill's method) [25]. The two second-order equations [Eqs. (46) and (47), and Eqs. (49) and (50)] for the amplitude and phase of each waveguide mode are converted into four first-order differential equations for computational convenience. Hence the system of equations to be solved consist of $6N_t+4N_w$ first-order differential equations, where N_t is the number of electrons and N_w the numbers of waveguide modes. Conservation of energy is tested at each axial position by comparing the efficiencies calculated with

$$\eta(z)=\langle\gamma(z)-\gamma_0\rangle/(\gamma_0-1)$$

and

$$\eta(z)=[P(z)-P_{\rm in}]/V_0I_0\ ,$$

where V_0 is the beam voltage and $P_{\rm in}$ is the input signal power. The power in the circuit $P(z)$ is calculated from Eq. (60). The conservation of energy is found to be satisfied to an accuracy of one part in 10^5.

The initial conditions on the beam are chosen to model an axisymmetric monoenergetic beam entering the interaction waveguide with a spatiotemporally modulated gyration angle $\phi=\phi_0-\xi z+pt$, as indicated in Eq. (1). Axial velocity spread of the electron beam is introduced through a Gaussian pitch-angle distribution of the form

$$f_0\sim\exp[-(v_z-v_{z0})^2/2(\Delta v_z)^2]\delta(\gamma-\gamma_0)$$

Initial conditions on the radiation field are chosen such that A_{mn} is at the noise level, $dA_{mn}/dz=0$, and $k_{z,mn}^2=(\omega^2/c^2-k_{mn}'^2)^{1/2}$.

The dependence of the rate of beam-wave energy transfer on the guiding-center location is determined by $J_{m-s}(k_{mn}'r_g)$. Hence efficient harmonic interaction for an axisymmetric beam ($r_g\to 0$) is absent unless $m=s$, as shown in Eqs. (8a), (8b), (48), (50), and (56). We will thus not consider any case where the cyclotron harmonic number and the azimuthal index number are not equal for all waveguide modes under consideration. Furthermore, we assume that operation is under matching conditions for strong interaction, as given in Eqs. (16)–(18). The matching conditions signify that the beam line and the waveguide dispersion curve are tangential; this is commonly termed the "grazing condition." At this point, the operating frequency and the cyclotron frequencies are connected to the cutoff frequency $\omega_{\rm cut}$ by

$$\omega=\gamma_{z0}\omega_{\rm cut}\ ,$$

$$s\Omega_0=seB_{\rm gr}/m_0=\gamma_0\omega_{\rm cut}/\gamma_{z0}\ ,$$

where $B_{\rm gr}$ is the grazing magnetic field and $\gamma_{z0}^2=(1-\beta_{z0}^2)^{-1}$.

Numerical results are shown for fifth-harmonic frequency converter at 94 GHz, as discussed in Sec. II B. The pump frequency $p=18.8$ GHz. The operating mode in the output section is a TE_{51} mode accumulating radiation at the fifth cyclotron harmonic ($s=5$), with parameters as given in Table I. The most dangerous competing modes are TE_{41} and TE_{61} at $s=4$ and 6, respectively. Power flow to the TM modes has been found to be negligible, even for conditions that depart from exact matching.

We first show the evolution of the design mode (TE_{51}) through the linear regime to saturation neglecting other competing modes. Efficiency as a function of interaction length is shown in Fig. 4 for a cold beam, i.e., $\delta v_z/v_{z0}=0$. For a uniform magnetic field $B=B_{\rm gr}$, the efficiency for fifth-harmonic generation is small as shown by the dashed curve in Fig. 4. The peak efficiency is 9.62% at an interaction length of 2.92 cm. All particles in the beam enter the interaction region at the same phase and the efficiency saturates as all particles slip out of synchronism with the wave due to energy depletion. However, the initial efficiency follows closely $2z^2\%$, the dependence found for this example from linear theory in Sec. II C. The efficiency may be greatly enhanced by tapering the magnetic field to maintain synchronism over a longer interaction time. The solid curve in Fig. 4 shows the enhancement of efficiency in a linearly tapered magnetic field; $B=B_{\rm gr}$ for $z<0.5R$ and $B=B_{\rm gr}[1-0.003(z-R)/R]$ for $z>0.5R$, where $B_{\rm gr}=7.983$ kG. These are the values which optimized the efficiency. In the tapered field the peak efficiency increases to 57.7% at an interaction length of 18.6 cm.

We now investigate the effect of mode competition on the saturation characteristics of the desired mode. The efficiency as a function of interaction distance is plotted in Fig. 5 for a cold beam in a linearly tapered B field

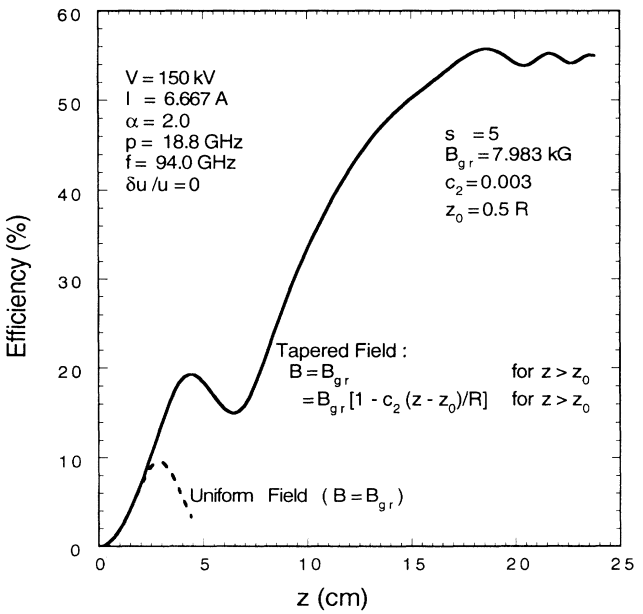

FIG. 4. Nonlinear efficiency for fifth-harmonic power generation in a uniform magnetic field (dashed curve) and a linearly tapered magnetic field (solid curve) for a cold beam. Parameters are as shown in figure.

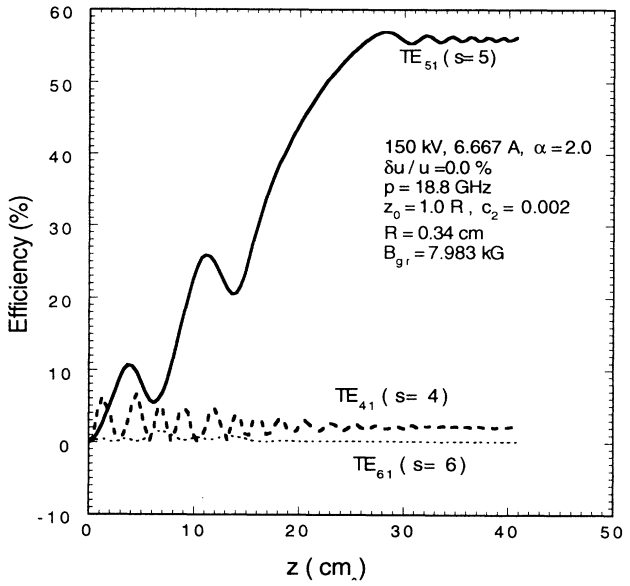

FIG. 5. Nonlinear efficiency for fourth-, fifth-, and sixth-harmonic power generation (acting simultaneously) for a cold beam and a linearly tapered magnetic field. Parameters are as shown in figure.

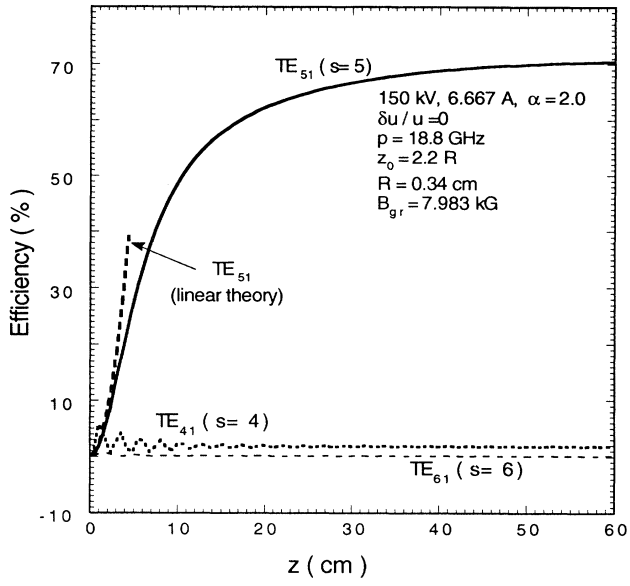

FIG. 6. Nonlinear efficiency for fourth-, fifth-, and sixth-harmonic power generation (acting simultaneously) for a cold beam and a nonlinearly tapered magnetic field. Parameters are as shown in figure.

when TE_{41}, TE_{51}, and TE_{61} modes are excited simultaneously. The magnetic field $B = B_{gr}$ for $z < R$ and $B = B_{gr}[1 - 0.002(z - R)/R]$ for $z > R$. The grazing condition is satisfied only by the operating mode (TE_{51} at $s = 5$). With these tapering parameters, the peak efficiency of the TE_{51} mode is found to be 57%, which is the same as in Fig. 4. However, the saturation length is increased to 28.3 cm, since some power flows to the TE_{41} mode initially. The efficiency of the TE_{41} mode increases to 6% at a distance of 4 cm. But beyond that point, the power gradually flows back to the fifth-harmonic TE_{51} mode as the sixth-harmonic efficiency settles down to about 2%. The TE_{61} mode barely grows above the noise level. Thus the TE_{51} mode attains a peak output power of 570 kW with negligible effect from the other two competing modes.

The linearly tapered B field is not the optimum for efficiency enhancement. This is illustrated in Fig. 6, where a nonlinear B-field taper is used to preserve the exact phase matching condition for the desired mode over the entire interaction length. Figure 6 also shows the efficiency $2z^2\%$ predicted from linear theory (see Sec. II B); it is evident that nonlinear effects cause the efficiency to fall below the linear prediction once the efficiency exceeds about 10%. Other factors influencing the startup of the growth are too small to show up on the scale of Figs. 4–6. No extended region of either quadratic or exponential growth is seen for this interaction. The magnetic field profile found is shown in Fig. 7. In this case a peak efficiency of 70.5% is found at a distance of 50.3 cm for a cold beam. The power flow to the two competing modes is negligible in this case also.

The effect of a spread in axial velocity of the particles is shown in Figs. 8 and 9. The saturated efficiency for the TE_{51} is plotted as a function of $\delta v_z / v_{z0}$ in Fig. 8 for the linearly tapered case. The efficiencies of the two competing modes are negligible and not shown. The efficiency drops from 57% to 40% as $\delta v_z / v_{z0}$ increase from 0 to 15%. A slight adjustment of the tapered parameters is necessary at each fractional velocity spread to maximize the efficiency. The effects of beam thermal effects on efficiency for the nonlinear B-field taper are

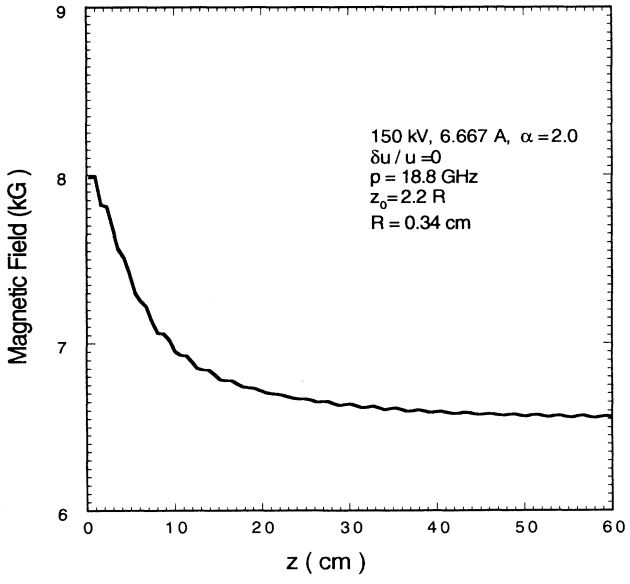

FIG. 7. Nonlinear magnetic field taper for the example shown in Fig. 6.

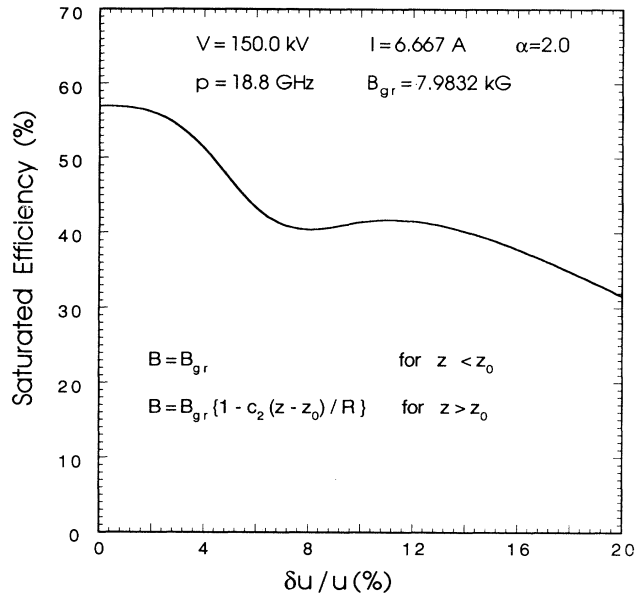

FIG. 8. Saturated efficiency for fifth-harmonic power conversion as a function of axial velocity spread for a linearly tapered magnetic field. Parameters are as shown in figure.

shown in Fig. 9. In this case, the efficiency decreases drastically with increase in the axial velocity spread. The synchronous conditions apply to all particles in a cold beam, but for a warm beam the conditions can be maintained only for a subset of the particles, which have been arbitrarily selected to be particles with $v_z = v_{z0}$ at $z = 0$.

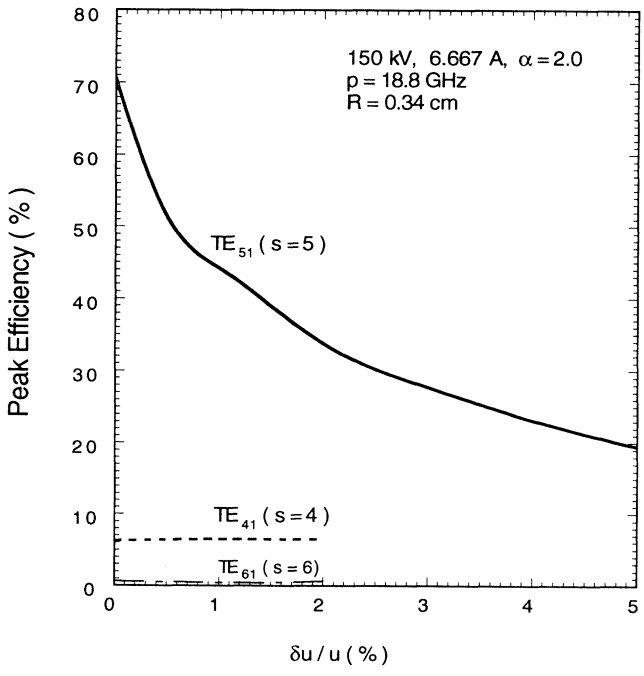

FIG. 9. Saturated efficiency for fourth-, fifth-, and sixth-harmonic power conversation as a function of axial velocity spread for a nonlinearly tapered magnetic field. Parameters are shown in figure.

The number of such particles decreases rapidly with increase in the axial momentum spread. For $\delta v_z / v_{z0} > 1\%$, the linearly tapered field gives higher efficiency than the nonlinearly tapered case considered in this paper.

V. CONCLUSIONS

A linear and nonlinear theory for the generation of gyroharmonic radiation from spatiotemporally modulated beams in cylindrical waveguides has been presented. Numerical results from the linear theory and particle simulation code results from the nonlinear theory have been given for fifth-harmonic generation of 94-GHz power using a 150-keV, 6.7-A beam. The main results of the theory can be summarized as follows:

(i) Power growth is absent from an axisymmetric beam at the mth temporal harmonic of the beam rotation frequency except for waveguide modes having an azimuthal mode index m. This greatly reduces the threat of mode competition at each harmonic, in contrast to the case with rectangular waveguides [2], where many waveguide modes can couple to the beam at each harmonic.

(ii) A beam with a uniform distribution of guiding centers will have a linearized mth harmonic power growth rate in the TE_{mn} mode no less than 90% that of a beam having no guiding-center spread if the ratio of the outer guiding-center radius R_b to the waveguide radius R is less than $0.8944/s'_{mn}$, where s'_{mn}, is the nth zero of $J'_m(s)$. For a fifth-harmonic device operating with a TE_{51} mode this reduces to $R_b/R < 0.1394$.

(iii) The diminution in linearized mth-harmonic power growth due to a uniform distribution of electron axial momentum will not be greater than 10% of the power growth rate for a cold beam if the normalized momentum spread is less than $48/N\%$, where N is the number of interaction guide wavelengths in the harmonic converter.

(iv) Power transfer from a cold beam to TM modes is absent under matching conditions, in which the beam axial velocity is equal to the group velocity for the TM mode. This results from an exact cancellation between contributions from the axial and transverse field components. For a beam with a small axial velocity spread, nonlinear simulations have shown negligible power transfer into TM modes as well. This fact diminishes further the threat from mode competition beyond what is stated in (i) above.

(v) Nonlinear particle simulations have shown that nearly 90% of the initial transverse energy on a cold beam can be converted to radiation at the fifth-harmonic of the beam rotation frequency if a tapered B field that preserves phase matching is used. Saturation is due to complete depletion of the transverse momentum of the electrons. For any other B-field taper (including no taper) saturation is due to particle slippage to a phase where wave growth is zero or negative. The spent beam is nearly monoenergetic, and the particles are all nearly in phase with one another. This indicates that a single-stage depressed collector could recover nearly all the residual beam energy, thus permitting the overall converter electronic efficiency to approach 100%.

(vi) For a fifth-harmonic converter, nonlinear simula-

tions have shown that conditions can be found where less tan 2% (0.5%) of the beam energy is converted to fourth-(sixth-) harmonic radiation. In addition, conditions can be found where all harmonics below a designated harmonic will be cut off, and thus cannot extract power from the beam. These results suggests that mode competition may not be a serious issue for converters designed in the parameter range for the examples shown in this paper.

(vii) For a linear B-field taper in a fifth-harmonic converter, a perpendicular efficiency of 71% has been found; this does not fall below 50% unless the relative axial velocity spread exceeds 14%. For the resonant B-field taper in a fifth-harmonic converter, a perpendicular efficiency of 88% has been found; this falls to below 40% for a relative axial velocity spread of greater than 1.0%. However, the efficiency calculations with finite-velocity spread were carried out for the same B-field profiles found to optimize power growth for a cold beam. It could be that a different taper would optimize power growth for each value of velocity spread, but this speculation has not been examined as yet.

In Ref. [13], a linear first order theory was derived for power transfer into an output cavity from a beam spun up at cyclotron resonance in short accelerator cavity. That theory accounted for temporal modulation imparted to the beam by the accelerator cavity fields in calculating power flow to the output cavity at the harmonic of the accelerator frequency. The power transfer was found to be proportional to $(\alpha L I_0 K_m / R)^2$, the same scaling found here. [see Eq. (20).] However, spatial modulation on the beam was not treated systematically, in an approximation reminiscent of theories of the gyroklystron [26], where spatial phase slip over a short output gap may not be significant. In a related work [27] by some of same workers as in [13], observations were made of eighth-harmonic gain in a traveling-wave interaction between a similarly spun-up beam and fields of a TE_{81} waveguide mode. However, the data were compared with a second-order theory invoking a dispersion relation that takes neither spatial nor temporal initial beam modulations into account. No justifications for overlooking the possibility of wave-number mismatch in the first work or the influence of initial spatiotemporal modulations on the beam in the second were given in these papers. We have thus concluded that the linear and nonlinear analysis presented in this paper could be important, not only for the design of future experiments, but for helping to understand past work as well.

Taken together, other results of this paper suggest that practical devices can be contemplated for production of millimeter wavelength radiation at power levels above and wavelengths below those that can be reached with conventional amplifiers or oscillators. The harmonic radiation would be phase locked to the rf source that drives the beam accelerator, but may exhibit only a small-frequency tunability due to the highly resonant nature of the process whereby power is transferred from the beam to the radiation. The converter output structure is a smooth-wall cylindrical waveguide, and the tapered magnetic field (for the 94-GHz example presented in this paper) can be produced with noncryogenic coils surrounding the waveguide. The analysis presented here omits any effects due to beam space charge, which could degrade the beam quality during the harmonic interaction and thereby decrease the interaction efficiency below the values found in this work. But if studies outside of the scope of the work described here can show that beam with sufficient quality in the parameter range required (150 keV, 7 A) can be produced, it could well be that a new class of millimeter wave sources may be possible.

ACKNOWLEDGMENTS

This work was supported by the Office of Naval Research, Office of Naval Technology, and by the U.S. Department of Energy.

[1] J. L. Hirshfield, Phys. Rev. A **44**, 6845 (1991).
[2] J. L. Hirshfield, Phys. Rev. A **46**, 5161 (1992).
[3] G. Caryotakis, in *Proceedings of the IEEE Particle Accelerator Conference, San Francisco, 1991* (IEEE, New York, 1991), p. 2928.
[4] K. E. Kreischer, T. L. Grimm, W. C. Guss, A. W. Mobius, and R. J. Temkin, Phys. Fluids B **2**, 640 (1990).
[5] P. B. Wilson, Bull. Am. Phys. Soc. **37**, 941 (1992).
[6] R. Prater, *et al.*, in *Proceedings of the 12th International Conference on Plasma Physics and Controlled Fusion, 1988, Nice* (IEAE, Vienna, 1989), Vol. I, p. 527.
[7] W. M. Manhaimer, Int. J. Electron. **72**, 1165 (1992).
[8] J. L. Hirshfield and J. M. Wachtel, Phys. Rev. Lett. **12**, 553 (1984); A. V. Gaponov, A. L. Gol'denberg, D. P. Grigor'ev, I. M. Orlova, T. B. Pankratova, and M. I. Petelin, Pis'ma Zh. Eksp. Teor. Fiz. **2**, 430 (1965) [JETP Lett. **2**, 267 (1965)].
[9] M. I. Petelin, Radiophys. Quantum Electron. **17**, 668 (1974); V. L. Bratman and G. G. Denisov, Int. J. Electron. **72**, 969 (1992).
[10] K. R. Chu, A. K. Ganguly, V. L. Granatstein, S. Y. Park, J. M. Baird, and J. L. Hirshfield, Int. J. Electron. **51**, 493 (1981); H. Guo, L. Chen, H. Keren, J. L. Hirshfield, S. Y. Park, and K. R. Chu, Phys. Rev. lett. **49**, 730 (1982).
[11] K. Yokoo, M. Razeghi, N. Sato, and S. Ono, Int. J. Electron. **67**, 485 (1989); A. K. Ganguly, S. Ahn, E. G. Zaidman, and A. S. Gilmour, Jr., IEEE Trans. Electron Devices **ED-38**, 2229 (1991).
[12] A. Fruchtman, Phys. Fluids B **4**, 4101 (1992).
[13] C. S. Kou, D. B. McDermott, N. C. Luhmann, Jr., and K. R. Chu, IEEE Trans. Plasma Science **PS-18**, 343 (1990).
[14] P. Malouf and V. L. Granatstein, Int. J. Electron. **72**, 943 (1992).
[15] G. S. Nusinovich and H. Li, Phys. Fluids B **4**, 1508 (1992).
[16] A. K. Ganguly and J. L. Hirshfield, Phys. Rev. Lett. **70**, 291 (1993).
[17] S. C. Zhang, Phys. Rev. A **45**, 1177 (1992).
[18] *Handbook of Mathematical Functions,* edited by M. Abramowitz and I. Stegen (Dover, New York, 1972), p. 363.
[19] *Handbook of Mathematical Functions* (Ref. [18]), p. 231.
[20] C. W. Roberson and P. Sprangle, Phys. Fluids B **1**, 3

(1989).
[21] A. K. Ganguly and S. Ahn, Int. J. Electron. **53**, 641 (1982).
[22] A. K. Ganguly and S. Ahn, Phys. Rev. A **42**, 3544 (1990).
[23] A. K. Ganguly, S. Ahn, and S. Y. Park, Int. J. Electron. **65**, 597 (1988).
[24] A. K. Ganguly and S. Ahn, Int. J. Electron. **67**, 261 (1989).
[25] *Handbook of Mathematical Functions* (Ref. [18]), p. 896.
[26] W. M. Bollen, A. H. McCurdy, B. Arfin, R. K. Parker, and A. K. Ganguly, IEEE Trans. Plasma Sc. **PS-13**, 417 (1985).
[27] D. S. Furuno, D. B. McDermott, C. S. Kou, N. C. Luhmann, Jr., and P. Vitelli, Phys. Rev. Lett. **62**, 1314 (1989).